DOI: 10.1002/chem.200500209

Topological Effects of a Rigid Chiral Spacer on the Electronic Interactions in Donor–Acceptor Ensembles

Dirk M. Guldi,*[a] Francesco Giacalone,[b] Gema de la Torre,[b] José L. Segura,[b] and Nazario Martín*[b]

In memoriam of Professor Christopher Foote

Abstract: Two triads (donor–spacer–acceptor), *ex*TTF–BN–C_{60} (**6**) and ZnP–BN–C_{60} (**7**), in which electron donors (i.e., *ex*TTF or ZnP) are covalently linked to C_{60} through a chiral binaphthyl bridge (BN), have been prepared in a multistep synthetic procedure starting from a highly soluble enantiomerically pure binaphthyl building block (**1**). Unlike other oligomeric bridges, with binaphthyl bridges, the conjugation between the donor and the acceptor units is broken and geometric conformational changes are facilitated. Consequently, distances and electronic interactions between the donor and C_{60} are drastically changed. Both donor–spacer–acceptor (D–s–A) systems (i.e., **6** and **7**) exhibit redox processes that correspond to all three constituent electroactive units, namely, donor, BN, and C_{60}. Appreciable differences were, however, observed when comparing triad **6**, in which no significant *ex*TTF–C_{60} interactions were noted, with D–s–A **7**, whose geometry favors donor–acceptor and π–π interactions that result in ZnP–C_{60} electronic communication. This through-space interaction is, for example, reflected in the redox potentials. Excited-state studies, carried out by fluorescence and transient absorption spectroscopy, also support through-space rather than through-bond interactions. Although both triads form the corresponding radical-ion pair, that is, exTTF$^{\bullet+}$–BN–$C_{60}^{\bullet-}$ and ZnP$^{\bullet+}$–BN–$C_{60}^{\bullet-}$, dramatic differences were found in their lifetimes: 165 μs and 730 ns, respectively.

Keywords: chiral spacers · electronic communication · fullerenes · porphyrinoids · tetrathiafulvalene

Introduction

Improving the understanding of electronic conduction through molecular-scale wires is a major challenge since it involves phenomena that are critical for major developments in the emerging field of "molecular electronics".[1] Recognizing the importance of this, concerted efforts have been directed in recent years towards the rational and systematic preparation of discrete organic molecules that promote the rapid and efficient transport of charge over long distances. Among these organic molecules, which all exhibit well-defined chemical structures, π-conjugated oligomers are particularly promising.[2] Thus, functionalized oligomers, ranging from oligo(phenyleneethynylene)s[3] and oligo(phenylenevinylene)[4] to oligothiophenes,[5] with a variety of functional end-groups have been developed to fine-tune the preparation of nanoscale materials for application in different fields.[6]

Recently, we reported on a series of donor–acceptor ensembles in which π-conjugated oligomeric building blocks of different conjugation length serve as "wires" to connect an electron-accepting [60]fullerene (C_{60}) with an electron-donating π-extended tetrathiafulvalene (*ex*TTF). In the corresponding monomeric-through-heptameric phenylenevinylene systems both redox-active components are located at the terminal positions of the oligomer. Photophysical studies carried out on these *ex*TTF–wire–C_{60} systems revealed 1) exceptionally low attenuation factors ($\beta \approx 0.01$ Å^{-1}) and 2) strong electronic coupling elements ($V \sim 5.5$ cm^{-1}) even at distances as large as 5 nm. Based on these findings we postulated that *ex*TTF–wire–C_{60} systems would exhibit molecular-wire behavior.[7] This earlier study has recently been extended to related donor–wire–C_{60} systems in which zinc

[a] Prof. Dr. D. M. Guldi
Institute for Physical and Theoretical Chemistry
University of Erlangen, 91058 Erlangen (Germany)
Fax: (+49) 9131-852-8307
E-mail: dirk.guldi@chemie.uni-erlangen.de

[b] Dr. F. Giacalone, Dr. G. de la Torre, Dr. J. L. Segura, Prof. Dr. N. Martín
Departamento Química Orgánica
Facultad de Ciencias Químicas, Universidad Complutense
28040-Madrid (Spain)
Fax: (+34) 913-944-103
E-mail: nazmar@quim.ucm.es

Supporting information for this article is available on the WWW under http://www.chemeurj.org/ or from the author.

tetrakis(di-*tert*-butylphenyl)porphyrinate (ZnP) functioned as the photoexcited electron donor. Despite the different electronic conjugation that exists, especially between the donor unit (ZnP) and oligomer moieties, slightly divergent nanowire behavior ($\beta \approx 0.03$ Å^{-1}) was manifested by the π-conjugated phenylenevinylene oligomer.[8]

In temperature-dependent measurements the charge recombination kinetics of both donor–wire–C_{60} systems (i.e., donor = *ex*TTF or ZnP) imply an efficient decoupling of the donor and acceptor moieties that leads to a significant slowdown in the rates of electron transfer. Reversible interruption of the π conjugation through temperature-induced rotation along the wire axis is thought to be responsible for this effect. An intriguing challenge lies in the incorporation of oligomeric building blocks that irreversibly break the π conjugation through, for example, the chemical nature of the oligomer. Chiral binaphthyl (BN) derivatives meet such criteria. They have also been used as electroactive species and, in contrast to π-conjugated phenylenevinylene oligomers, the π conjugation between the two naphthyl units is efficiently disrupted by the existing atropisomerism.[9]

By using soluble BN we have targeted the synthesis of a series of π-conjugated polymers with well-balanced control over the effective conjugation length spanning the BN units.[10] The use of BN systems as nonconjugated donor–acceptor bridges has not been addressed or explored to date despite the strong impact that we expect from its presence on the electronic features of donor–BN–acceptor ensembles. Therefore, we describe herein for the first time two new donor–bridge–acceptor systems, *ex*TTF–BN–C_{60} and ZnP–BN–C_{60}, in which both electron donors are covalently linked to C_{60} through BN groups. In order to increase the solubility of these systems, the BN groups bear solubilizing alkoxy chains. In contrast to previous systems, the BN groups facilitate geometric conformational changes that impact on the electron donor–acceptor interactions in the resulting ensembles. The effects on the stabilization of the photogenerated radical-ion pairs are particularly pronounced.

Abstract in Spanish: *Se han preparado dos tríadas (Dador-Espaciador-Aceptor) exTTF–BN–C_{60} (**6**) y ZnP–BN–C_{60} (**7**), empleando una estrategia sintética en varios pasos a partir de unidades solubles de binaftilo enantiomericamente puro. En dichas tríadas los dadores de electrones (exTTF o ZnP) están unidos covalentemente al C_{60} a través de un puente de binaftilo quiral. A diferencia de otros espaciadores oligoméricos, en los BN la conjugación entre las unidades dadora y aceptora se encuentra interrumpida y se facilitan los cambios en la geometría conformacional. Por consiguiente, tanto las distancias como las interacciones electrónicas entre el dador y el C_{60} cambian de manera drástica. Ambas tríadas D–s–A (**6** y **7**) dan lugar a los procesos redox correspondientes a las tres unidades electroactivas, es decir dador, BN y C_{60}. Sin embargo, se observaron diferencias apreciables al comparar la tríada **6**, en la que no se detectan interacciones exTTF–C_{60}, con el sistema D–s–A **7**, donde la geometría favorece tanto las interacciones dador–aceptor, como las interacciones π–π que dan lugar a una comunicación electrónica ZnP–C_{60}. Estas interacciones a través del espacio se reflejan, por ejemplo, en los potenciales redox. Estudios en estado excitado, llevados a cabo mediante espectroscopia de fluorescencia y de absorción con resolución temporal, apoyan las interacciones a través del espacio frente a las interacciones a través de enlace. Aunque ambas tríadas forman el par ion radical, es decir, exTTF$^{\bullet+}$–BN–$C_{60}^{\bullet-}$ y ZnP$^{\bullet+}$–BN–$C_{60}^{\bullet-}$, se han encontrado diferencias notables en sus tiempos de vida media, de 165 μs y 730 ns, respectivamente.*

Results

Synthesis and characterization: To prepare the target compounds *ex*TTF–BN–C_{60} (**6**) and ZnP–BN–C_{60} (**7**), several molecular building blocks were synthesized following previously described procedures.[8,11–13] The synthesis of formyl-functionalized enantiomerically pure binaphthyl moiety **1** was achieved through the bromination of (*R*)-1,1′-bi-2-naphthol at the 6,6′-positions and subsequent *o*-alkylation with dodecyl bromide. The product so-obtained was then treated with *n*BuLi and DMF to afford compound **1**.[12] Triphenylphosphonium-containing extended-TTF **2** was prepared from the corresponding 2-hydroxymethyl derivative, which, in turn, was obtained through a multistep synthetic procedure.[11] Finally, treatment of zinc(II) bromomethylporphyrinate[13] with $P(OMe)_3$ led to dimethylphosphonate porphyrin derivative **3**.[8] The single chromophore zinc(II) tetrakis(di-*tert*-butylphenyl)porphyrinate (ZnP) and *ex*TTF were also prepared as reference compounds.

Scheme 1 summarizes the preparation of the intermediate systems *ex*TTF–BN (**4**) and ZnP–BN (**5**). The Wittig reaction between phosphonium salt **2** and an excess of dialdehyde **1** using potassium *tert*-butoxide as a base gave **4** in 51% yield. Similarly, conversion of phosphonate-containing porphyrin **3** and binaphthyl-dialdehyde **1** into **5** was achieved through a Wittig–Horner olefination reaction in 68% yield. Both processes gave rise to minute amounts of the symmetrical *ex*TTF–BN–exTTF and ZnP–BN–ZnP systems, respectively, which were separated from the corresponding target systems (i.e., **4** and **5**) by column chromatography.[14]

The D–s–A systems **6** and **7** were prepared by the Prato reaction,[15] namely, by cycloaddition between **4** or **5**, *N*-octylglycine, and C_{60} in chlorobenzene, in 37 and 47% yields, respectively (Scheme 1). Owing to the presence of dodecyloxy chains on the BN moiety as well as the octyl chain on the pyrrolidine ring both triads are sufficiently soluble in common organic solvents to allow their spectroscopic, electrochemical, and photophysical characterization. Note that **6** and **7** are not pure enantiomers but diastereoisomers since chiral centers have been created at the fulleropyrrolidine rings. However, high-resolution ^{1}H and ^{13}C NMR spectroscopy (500 MHz) was not sensitive enough to distinguish between the diastereomers.

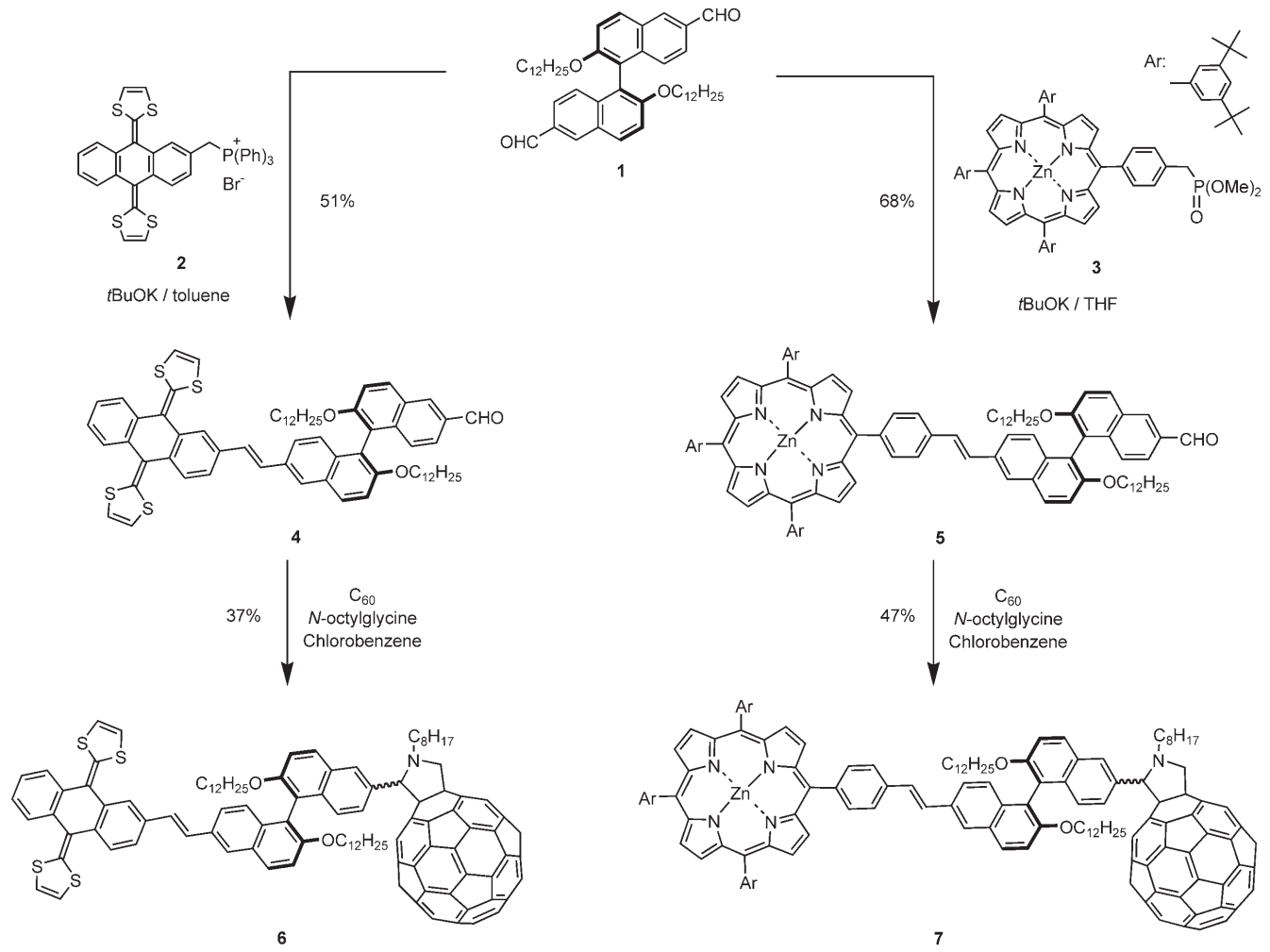

Scheme 1. Synthesis of triads **6** and **7**.

All structures were validated by spectroscopic analyses. For example, the ^{1}H NMR spectrum of **6** shows a distinctive singlet at $\delta = 6.30$ ppm, which corresponds to the protons located in the dithiole rings. Similarly, a typical AB system, corresponding to the *trans* olefinic protons, was observed for **6** at around $\delta = 7.3$ ppm ($J \approx 16$ Hz). The spectrum of **7** exhibits a multiplet at around 9 ppm which arises from porphyrinic pyrrole protons. The pyrrolidine signature appears in the spectra of both **6** and **7** as two doublets and one singlet between $\delta = 3.8$ and 5.2 ppm. For **7** the second doublet is overlapped by OCH_2 protons between $\delta = 3.7$ and 4.0 ppm. Finally, the proposed structures were confirmed by high-resolution mass spectrometry.

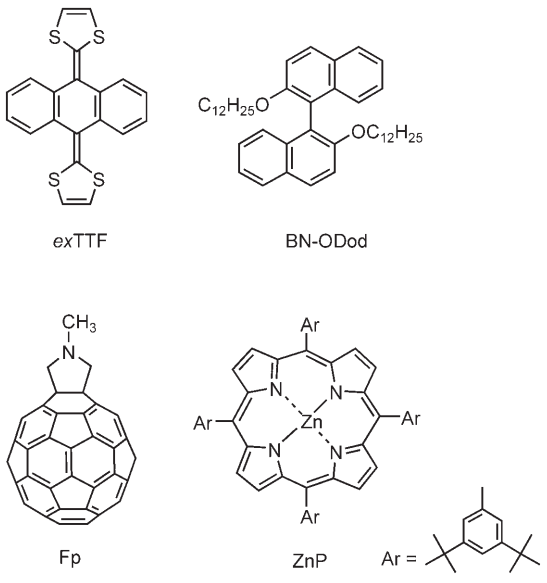

Electrochemistry: The electrochemical features of **6** and **7** were probed by cyclic voltammetry at room temperature (see Figure 1). Their redox potentials are collected in Table 1, along with those of the reference systems ZnP, *ex*TTF, 2,2′-bis(dodecyloxy)-1,1′-binaphthalene (BN–ODod), fulleropyrrolidine (Fp), and pristine C_{60}.

Compounds **6** and **7** exhibited amphoteric redox behavior, namely, several oxidation and reduction steps. In particular, both exhibit four reduction waves corresponding to the first four reduction steps of the fulleropyrrolidine unit, which are

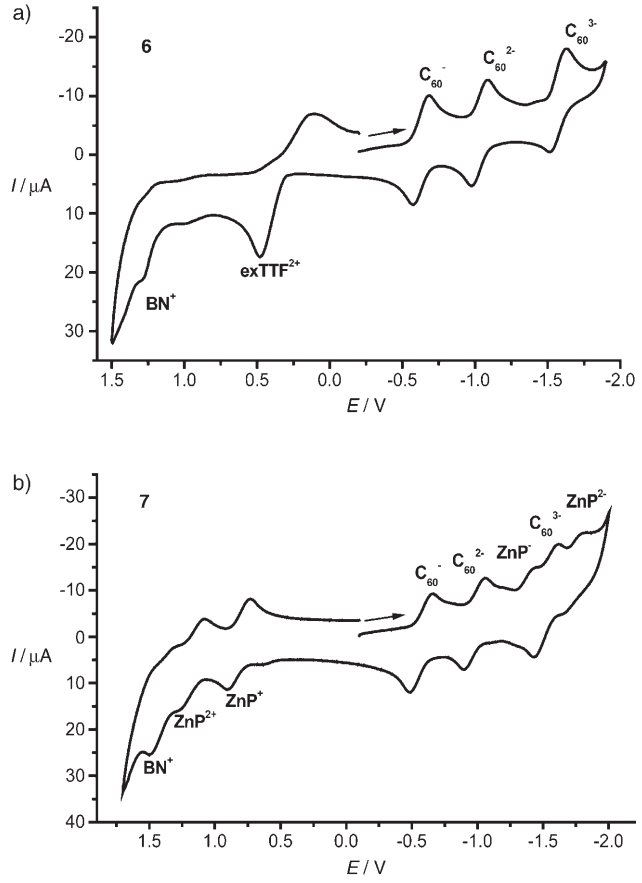

Figure 1. Cyclic voltammograms for a) compound **6** and b) compound **7** at room temperature (solvent: *o*DCB/MeCN 4:1 v/v; supporting electrolyte: Bu_4NClO_4; scan rate = 200 mV s^{-1}). Only three waves are shown for the C_{60} moiety (see the Supporting Information for full details of reduction).

cathodically shifted relative to those of pristine C_{60}. This behavior has been attributed to the saturation of a double bond in the fullerene unit, which raises the LUMO energy.[16] For triad **7**, two additional reduction waves were registered at −1.42 and −1.79 V, which correspond to the redox processes of the ZnP moiety[17] (Figure 1b).

Both triads exhibited oxidation waves that correspond to the donor unit as well as to the alkoxy-substituted BN moiety.[12,18] For example, **6** shows a first oxidation wave at 0.57 V corresponding to the *ex*TTF moiety and two additional waves at 1.04 and 1.33 V assigned to BN. The oxidation wave of the *ex*TTF group in **6** is somewhat shifted relative to that of the *ex*TTF reference as a result of the chemical functionalization of the *ex*TTF moiety. Triad **7** exhibits the first two oxidation waves of ZnP at 0.89 and 1.25 V, while BN is oxidized at about 1.45 V. In **7**, the first oxidation wave of BN is masked by the ZnP oxidation.

A closer inspection of Table 1 reveals several interesting trends. In **7**, both oxidation and reduction waves are slightly shifted, relative to the reference systems, towards more positive and negative potentials, respectively. Trends like this suggest charge-transfer behavior in which the electron density is partially shifted from the electron donor (i.e., ZnP) to the electron acceptor (i.e., C_{60}). On the basis of the same redox potential analysis, no significant electronic interactions are found for the ground state of **6**.

Molecular geometry: Owing to the rotational freedom of the naphthyl–pyrrolidine linkage we determined the geometry of ZnP–BN–C_{60} (**7**) and *ex*TTF–BN–C_{60} (**6**) by theoretical calculations at the semiempirical PM3 level. For ZnP–BN–C_{60} (**7**) we found two conformers, namely, I and II, which are characterized by a folded and a stretched linear geometry, respectively. Both are illustrated in Figure 2. Notably, conformer I is 1.2 kcal mol^{-1} more stable than conformer II. A characteristic of conformer I is the close proximity of the electron donor (ZnP) and the electron acceptor (C_{60}). Such geometries open the way for appreciable through-space–through-solvent electronic interactions. On the other hand, three conformers (i.e., I, II, and III) emerged for the *ex*TTF–BN–C_{60} system, including two that could be considered equivalents of conformers I and II of the ZnP–BN–C_{60} system (see Figure 2). However, none of the three conformers showed thermodynamic selectivity. Note that our calculations were based on a comparison of features such as binding energy or heat of formation, which led overall to marginal differences of less than 0.6 kcal mol^{-1} (relative stability I > III > II).

We have also calculated the HOMO and LUMO topologies corresponding to the minimum-energy conformations determined for compounds **6** and **7** (Figure 3). Note that, as expected, the LUMO is localized only on the C_{60} electron-acceptor unit in **6** and **7**. However, there is a significant difference between the HOMOs of the two molecules. Thus, compound **6** exhibits an HOMO that is delocalized over the *ex*TTF electron-donor unit and the adjacent naphthyl unit of the binaphthyl system with larger coefficients on the central *ex*TTF moiety, which perfectly supports the electrochemical findings as well as the electronic communication through the π-conjugated

Table 1. Redox potentials of novel compounds **6** and **7** and reference compounds.[a]

Compound	E^1_{pa}	E^2_{pa}	E^3_{pa}	E^1_{pc}	E^2_{pc}	E^3_{pc}	E^4_{pc}	E^5_{pc}	E^6_{pc}
*ex*TTF	0.55	–	–	–	–	–	–	–	–
ZnP	0.84	1.23	–	−1.42	−1.78	–	–	–	–
BN–ODod	1.51	–	–	–	–	–	–	–	–
C_{60}	–	–	–	−0.54	−0.96	−1.43	−1.92	–	–
Fp[b]	–	–	–	−0.64	−1.03	−1.58	−1.99	–	–
6	0.57	1.04	1.33	−0.64	−1.05	−1.60	−2.09	–	–
7	0.89	1.25	1.45	−0.65	−1.05	−1.42	−1.60	−1.79	−2.07

[a] V versus SCE; working electrode: GCE; reference electrode: Ag/Ag^+; counter electrode: Pt; 0.1 M Bu_4NClO_4; scan rate: 200 mV s^{-1}; concentration: 0.5–2.0 × 10^{-3} M; solvent: *o*DCB/MeCN (4:1 v/v). Values were determined within the experimental error of ±5 mV. [b] Fp: *N*-methylpyrrolidino[3,4:1,2][60]fullerene.

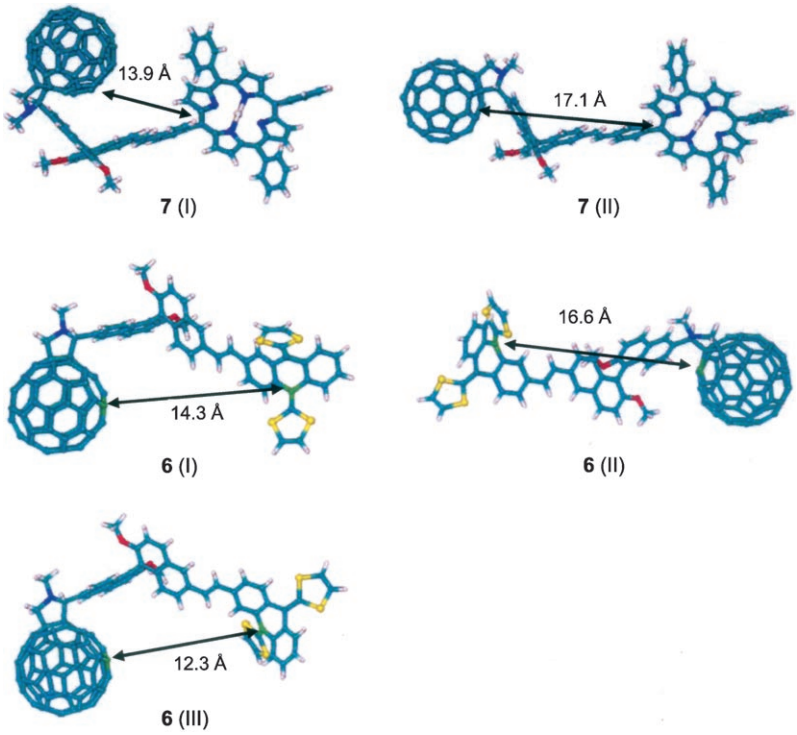

Figure 2. Most stable conformers determined for compounds **7** (I and II) and **6** (I, II and III) by semiempirical calculations (PM3). The numbers represent the edge-to-edge distance between C_{60} and the donor unit. Dodecyl groups were substituted with methyl groups for the computational study.

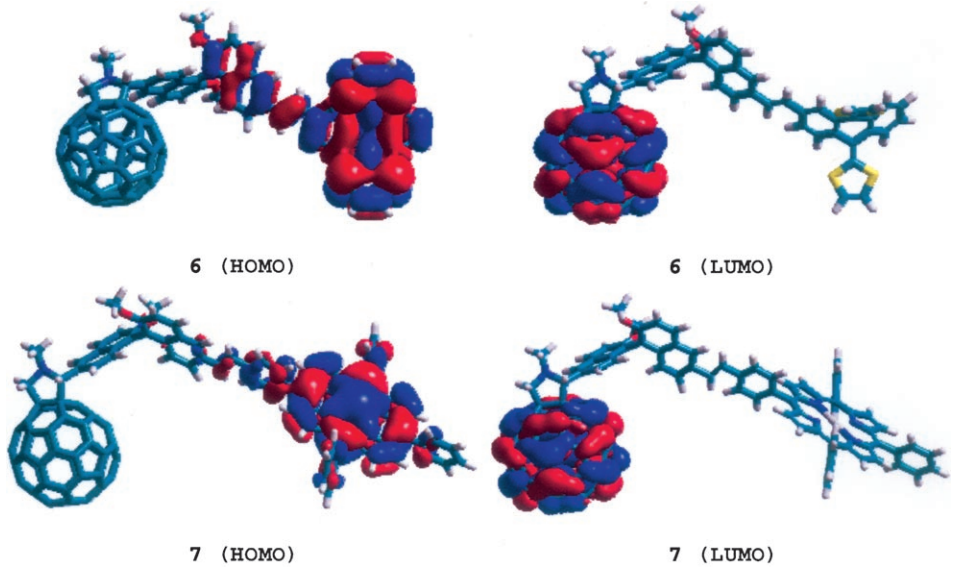

Figure 3. HOMO and LUMO topologies of the minimum-energy conformations determined for triads **6** and **7**.

vinyl linkage that exists between the *ex*TTF and naphthyl units. In contrast, the HOMO of the donor–spacer–acceptor system **7** is mainly localized on the ZnP electron-donor unit with a small contribution from the adjacent naphthyl moiety which has, relative to **6**, smaller coefficients over the naphthyl unit (see Figure 3). This difference can be attributed to the dihedral angle of 68° between the phenyl group and the porphyrin in **7**.[19]

Absorption spectroscopy: Compared with the absorption spectra of the individual building blocks, that is, BN, ZnP, *ex*TTF, and Fp, the spectra of ZnP–BN–C_{60} (**7**) and *ex*TTF–BN–C_{60} (**6**) deviate appreciably from the strictly linear superimposition of the individual components (see Figure 4). In particular, BN exhibits transitions at 234, 282, and 339 nm. The spectrum of ZnP consists of two sections: 1) the Soret band with a maximum at 424 nm and 2) the Q band with maxima at 551 and 590 nm. For *ex*TTF a maximum is recorded at 431 nm, while Fp's strongest bands are at 220, 265, and 330 nm and extend all the way to the energetically lowest-lying transition at around 690 nm. Unmistakably, Figure 4b illustrates that in **7** the ZnP-centered transitions (i.e., the Soret and Q bands) are slightly shifted to the red (2 nm for the Soret band). Again, this finding suggests a kind of electron-donor–electron-acceptor interaction.[20] Also the spectrum of **7** (Figure 4a) is different to that of the individual components: The λ_{max} for **6** is slightly bathochromically shifted (~5 nm for the *ex*TTF moiety).[21] This is primarily accounted for by the π conjugation that exists between the *ex*TTF unit and the adjacent naphthalene moiety.

In summary, electrochemistry, molecular modeling, and ground-state features suggest the presence of weak electronic donor–acceptor interactions in **7**, which could be driven by the flexibility of BN and charge-transfer interactions. Note there are plenty of precedents for interacting ZnP/C_{60}, covalent and noncovalent, ensembles.[22] In **6**, on the other hand, such interactions appear to be absent, owing to the mismatching geometric needs of *ex*TTF and C_{60} (vide infra).

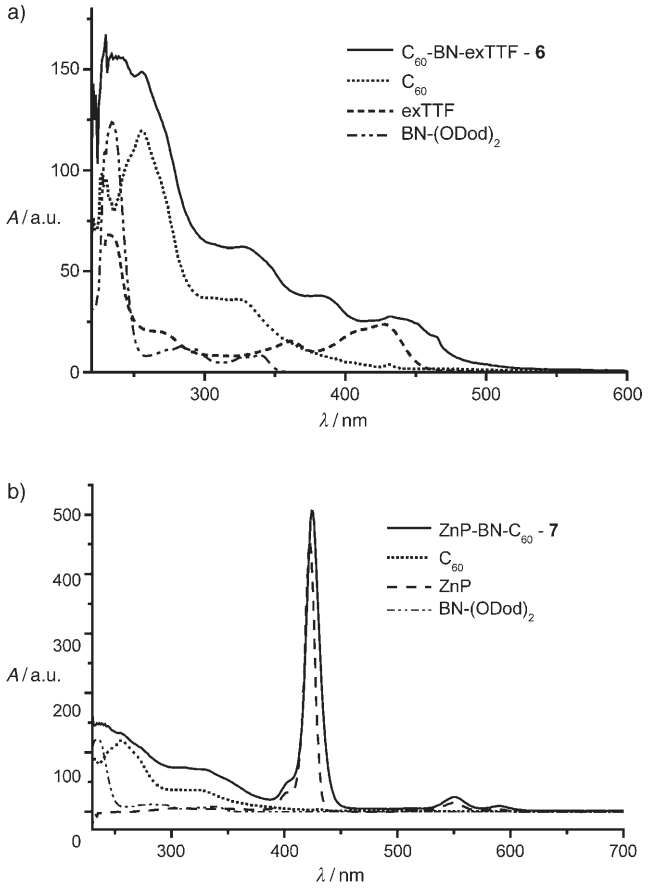

Figure 4. a) UV/Vis spectra of **6** and its molecular components *ex*TTF, BN–ODod (2,2′-bis[dodecyloxy)-1,1′-binaphthalene], and Fp used as reference; b) UV/Vis spectra of **7**, ZnP, BN–ODod, and Fp in dichloromethane.

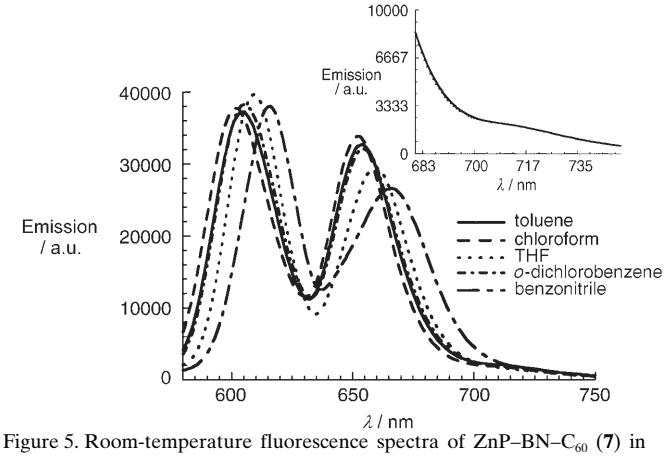

Figure 5. Room-temperature fluorescence spectra of ZnP–BN–C_{60} (**7**) in different solvents (see label for assignment) recorded with solutions that exhibit optical absorptions of 0.5 at the 425 nm excitation wavelength. Insert shows an amplification of the fluorescence spectrum in toluene.

Fluorescence spectroscopy: Steady-state and time-resolved fluorescence spectra of dilute ZnP–BN–C_{60} solutions reveal a solvent-independent deactivation of the ZnP fluorescent state: Regardless of the solvent polarity the fluorescence quantum yield ($8.0\pm0.2\times10^{-3}$) remained constant. This is shown in Figure 5 and does not vary notably with excitation wavelength (i.e., 425 or 560 nm). Note that these quantum yields, relative to the ZnP reference, reflect a fluorescence quenching of around 80%. Similarly, the ZnP fluorescence was found to have the same short lifetime (i.e., $0.32\pm$ 0.02 ns) when fluorescence decay was measured at 605 or 655 nm in toluene, THF, and benzonitrile.

A first insight into product formation was possible after amplifying the 700–750 nm region, which in toluene revealed the signature of fullerene fluorescence (see the insert to Figure 5).[23] A quantum yield of $5.0\pm0.5\times10^{-4}$ indicates that a nearly quantitative (i.e., ~80%) transduction of the singlet excited state, funneling the excitation light from the ZnP chromophore (2.1 eV) to C_{60} (1.76 eV), had occurred. Although the fullerene signature only appears as a weak shoulder, it is still important to verify that this feature is missing in the more polar solvents. In parallel experiments, we tested the C_{60} fluorescence lifetime at 725 nm. Here the fluorescence time-profiles were bi-exponential with a short- (~0.4 ns) and a long-lived component (~1.5 ns). While the former component corresponds to the quenched ZnP fluorescence, the latter corresponds to the intrinsic and unquenched fluorescence lifetime of C_{60}.

No direct product assignment was possible in more polar solvents. However, the absence of any notable fullerene fluorescence suggests electron-transfer quenching occurs which yields a charge-separated radical-ion pair. Note that the binaphthyl building block, with two independent naphthalene units, is ruled out as an active redox component and, therefore, serves exclusively as a bridging unit.

In *ex*TTF–BN–C_{60}, which was excited at 335 nm, we noted very different fluorescence behavior. Experiments in a variety of solvents (see Figure 6) indicated that the fluorescence of the C_{60} building block (i.e., Fp) was quenched. As the polarity increases (i.e., toluene, chloroform, and THF) the fluorescence weakens. Going beyond this point, namely, dichloromethane, *o*-dichlorobenzene, and benzonitrile, the fluorescence starts to increase again. We ascribe this trend to repulsive forces in the *ex*TTF/C_{60} couple that are aug-

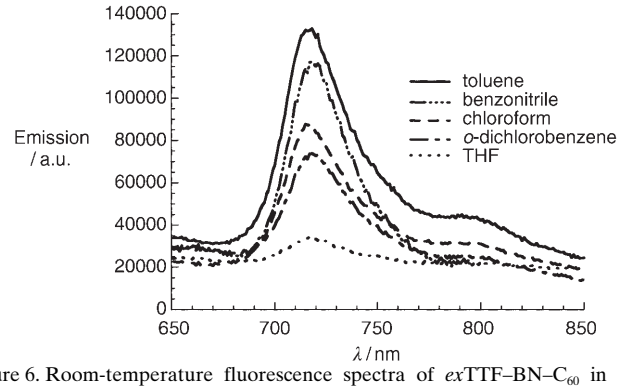

Figure 6. Room-temperature fluorescence spectra of *ex*TTF–BN–C_{60} in different solvents (see label for assignment) recorded with solutions that exhibit optical absorptions of 0.5 at the 337 nm excitation wavelength.

mented by the properties of the solvents. A similar trend was observed in the fluorescence decay measurements.

Transient absorption spectroscopy: Conclusive information about the photoproducts came from transient absorption spectroscopy. In particular, with the help of short laser pulses (i.e., 18 ps or 8 ns) at 532 nm, which corresponds to the region in which one of the Q-band transitions is a maximum, or 355 nm, at which C_{60} absorbs, the fate of the ZnP and C_{60} singlet excited states was probed.

ZnP and C_{60} references: In a reference experiment with the ZnP building block two transients were discerned on the pico- and nanosecond time scale. The first transient, which appeared simultaneously with the conclusion of the picosecond laser pulse, has been assigned to the short-lived singlet excited state, ^{1}*ZnP.[24] Spectral characteristics of ^{1}*ZnP are minima in the Q-band region and a broad transition in the 600–750 nm range. Fast and efficient intersystem crossing between the singlet and triplet states is responsible for the short singlet lifetime of 2.3 ns. The second transient, namely, the triplet excited state, appeared on the picosecond time scale as a slowly evolving species, while on the nanosecond scale its formation is virtually instantaneous.[24] The most important signature of the ZnP triplet is a maximum at around 860 nm (see Figure 7).

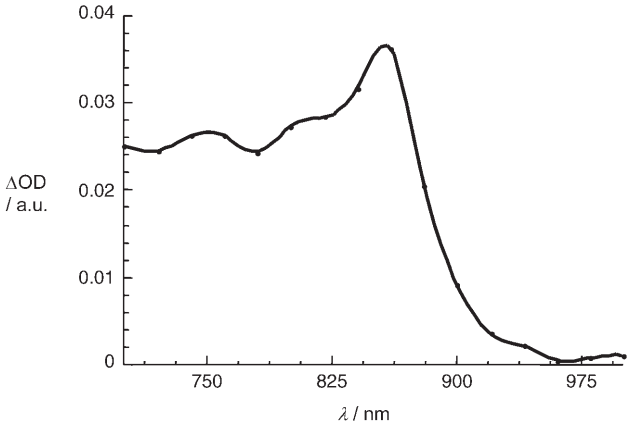

Figure 7. Differential absorption spectrum (near-infrared) obtained upon nanosecond flash photolysis (355 nm) of $\sim 1.0\times10^{-5}$ M solutions of ZnP in nitrogen-saturated toluene with a time delay of 50 ns at room temperature. The spectrum corresponds to the triplet–triplet spectrum of the ZnP chromophore.

Similarly, singlet and triplet transitions were recorded for the C_{60} building block (i.e., Fp). While the singlet excited-state absorption maximum at 880 nm, in the form of a rather broad band, was found instantly after the picosecond excitation, the much slower generated triplet exhibits the following characteristics: Maxima at 360 and 700 nm and a shoulder at 800 nm (not shown).

ZnP–BN–C_{60}: With ZnP–BN–C_{60}, differential absorption changes recorded immediately after the laser pulse include Q-band minima and maxima in the 600–750 nm range. This observation is crucial, since it attests the exclusive formation of the ZnP singlet excited state in ZnP–BN–C_{60}.

In toluene, two distinct follow-up reactions occur after the completion of the initially formed ^{1}*ZnP. The first process is a fast decay, which is essentially complete 500 ps after the laser pulse, and has a rate constant of $2.5\pm0.2\times10^9$ s^{-1}. In contrast, the second, slower step is a grow-in process with a time constant of 1.8 ns ($5.5\pm0.5\times10^8$ s^{-1}). Spectral analysis of the two transients formed in toluene, after 500 and 4000 ps, shows that the first-formed species has a broad band in the 850–950 nm range. These spectral characteristics are similar to those noted for the C_{60} singlet excited-state absorption.[23] On the other hand, the slower produced transient exhibits the characteristics of the C_{60} triplet excited state, that is, a maximum at 700 nm. Consequently, we can conclude that a long-range singlet–singlet energy transfer, occurring by a dipole–dipole mechanism, governs the deactivation of the photoexcited ZnP. In line with this energy-transfer mechanism, the differential absorption changes recorded immediately after a 20 ns pulse showed the spectral features of the C_{60} triplet excited state—two maxima located at 360 and 700 nm and a low-energy shoulder at around 800 nm—formed in nearly quantitative yields.

The picture is different in THF and benzonitrile. Instead of seeing the transduction of singlet excited-state energy, which ZnP–BN–C_{60} exhibits in toluene, the singlet–singlet features decay through an intramolecular electron-transfer reaction. Spectroscopic proof for the formation of a radical-ion pair was obtained from the features that developed in parallel with the disappearance of the ZnP singlet–singlet absorption, which is exemplified in Figure 8.

In the visible region, the broad absorption in the 600–700 nm region corresponds to the one-electron oxidized $ZnP^{\bullet+}$,[25] while in the near-infrared region the maximum at

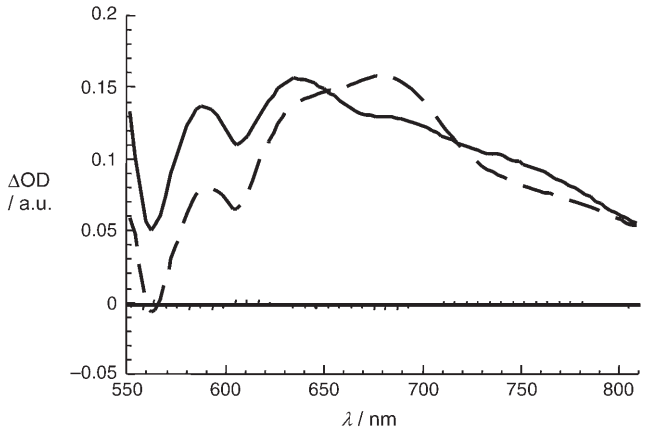

Figure 8. Differential absorption spectra (visible and near-infrared) obtained upon picosecond flash photolysis (532 nm) of $\sim 1.0\times10^{-5}$ M solutions of ZnP–BN–C_{60} in nitrogen-saturated THF with a time delay of −50 ps (dotted spectrum), +50 ps (solid spectrum), and 4000 ps (dashed spectrum) at room temperature. The spectra correspond to the changes that are associated with the formation and subsequent transformation of the ZnP singlet excited state to the radical ion pair, $ZnP^{\bullet+}$–BN–$C_{60}^{\bullet-}$.

1000 nm resembles the signature of the one-electron reduced $C_{60}^{\bullet-}$.[26] Both radical-ion-pair attributes (see Figure 9) are stable on the picosecond time scale and start to decay slowly in the nanosecond regime in most solvents. Time–absorption profiles illustrate that $ZnP^{\bullet+}$–BN–$C_{60}^{\bullet-}$ decays in a single step with radical-ion-pair lifetimes in THF, *o*-dichlorobenzene, and benzonitrile that are, however, quite short with values of 1090, 980, and 730 ns, respectively.

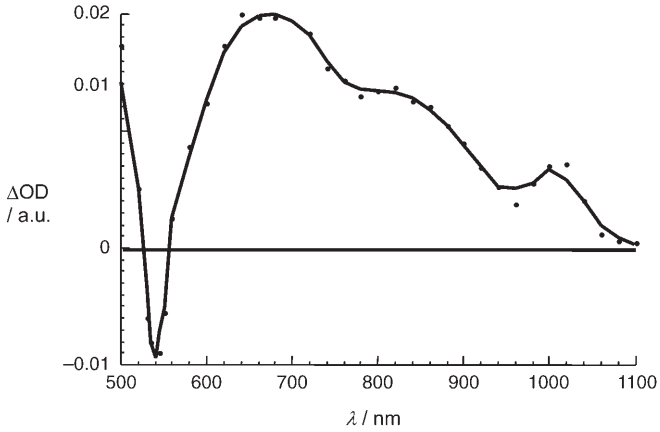

Figure 9. Differential absorption spectrum (visible and near-infrared) obtained upon nanosecond flash photolysis (532 nm) of $\sim 1.0\times10^{-5}$ M solutions of ZnP–BN–C_{60} in nitrogen-saturated THF with a time delay of 50 ns at room temperature. The spectrum corresponds to the radical-ion-pair spectrum of $ZnP^{\bullet+}$–BN–$C_{60}^{\bullet-}$.

As can be seen from Figure 10, a residual $ZnP^{\bullet+}$–BN–$C_{60}^{\bullet-}$ radical-ion-pair absorption of less than 5% was seen on a time scale of more than 5 μs.

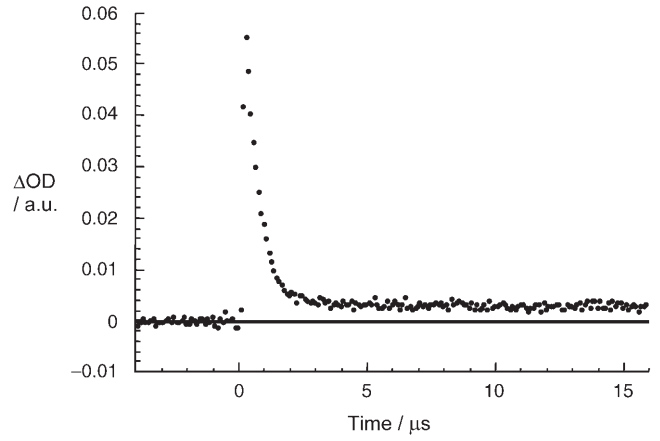

Figure 10. Time–absorption profile at 1000 nm, monitoring the $C_{60}^{\bullet-}$ decay dynamics of $ZnP^{\bullet+}$–BN–$C_{60}^{\bullet-}$ produced upon 532 nm excitation in nitrogen-saturated benzonitrile.

exTTF–BN–C₆₀: In the picosecond transient absorption measurements, when exciting *ex*TTF–BN–C_{60} with 355 nm laser pulses, the differential absorption changes that we recorded immediately after the excitation resemble those of photoexcited C_{60}. In particular, the 880 nm band corresponds to the singlet–singlet transition of C_{60}. Again this confirms, despite the presence of *ex*TTF, the successful formation of the C_{60} singlet excited-state. Unlike ZnP–BN–C_{60}, the initial singlet excited state was subject to solvent-dependent decay.

The product of the initial decay is the metastable $(exTTF)^{\bullet+}$–BN–$C_{60}^{\bullet-}$ radical-ion pair, which exhibits the attributes of the one-electron oxidized *ex*TTF moiety ($\lambda_{max}\sim$ 665 nm)[27] and that of the one-electron reduced fullerene ($\lambda_{max}\sim$1000 nm). Figure 11 shows these absorption changes. It is only after 6 ns laser excitation that the $(exTTF)^{\bullet+}$–BN–$C_{60}^{\bullet-}$ transient starts to decay.

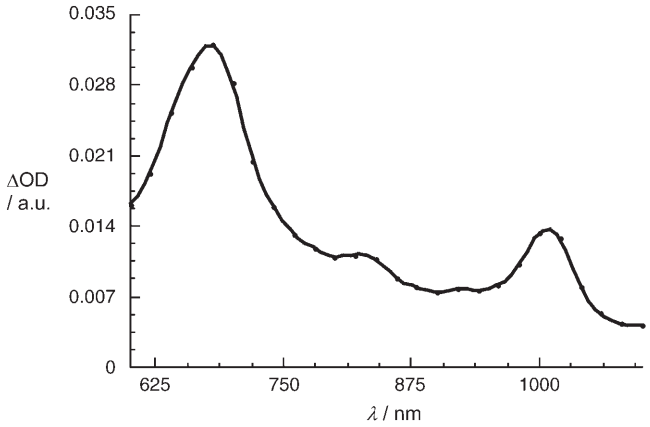

Figure 11. Differential absorption spectrum (visible and near-infrared) obtained upon nanosecond flash photolysis (337 nm) of $\sim 1.0\times10^{-5}$ M solutions of *ex*TTF–BN–C_{60} in nitrogen-saturated THF with a time delay of 50 ns at room temperature. The spectrum corresponds to the radical-ion pair, $exTTF^{\bullet+}$–BN–$C_{60}^{\bullet-}$.

In THF, the decay dynamics of the radical-ion-pair absorption, as typically recorded on the nanosecond/microsecond time scale, reveal a two-component decay (Figure 12a). The faster decaying segment has a lifetime of 2.2 μs, while that of the slower decaying segment lies in the range of several tens of microseconds, 63 μs to be exact. Both decay components were best fitted by first-order kinetics, confirming intramolecular reactions. Determination of the quantum yields of charge separation for the two radical-ion pairs led to the conclusion that the short- and long-lived radical-ion pairs are formed in an 8:2 ratio. In *o*-dichlorobenzene the lifetime of the short-lived component is 0.95 μs.

The same $(exTTF)^{\bullet+}$–BN–$C_{60}^{\bullet-}$ radical-ion pair evolves in benzonitrile. In contrast with the case in THF, in benzonitrile we see 10% of the fast and 90% of the slow decaying component (see Figure 12b). First-order kinetic analysis revealed a lifetime of 165 μs, which indicates remarkable radical-ion-pair stability.

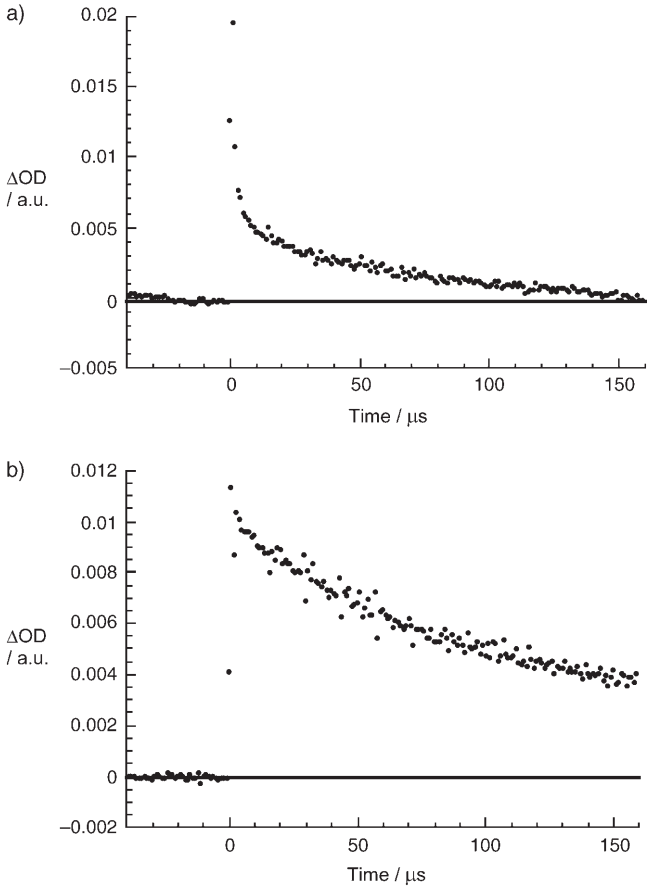

Figure 12. Time–absorption profiles at 1000 nm, monitoring the $C_{60}^{\bullet-}$ decay dynamics of *ex*TTF$^{\bullet+}$–BN–$C_{60}^{\bullet-}$ produced upon 337 nm excitation in nitrogen-saturated a) THF and b) benzonitrile.

Discussion

We have designed two novel donor–acceptor ensembles, ZnP–binaphthyl–C_{60} (**7**) and *ex*TTF–binaphthyl–C_{60} (**6**), in which a rigid bridging unit (i.e., chiral binaphthyl) was incorporated. The dihedral angle (~64°) at which the two naphthyl units are aligned with respect to each other is important. This provides a rigid framework to switch between two different conformational geometries. Simple rotation along the naphthyl–pyrrolidine linkage allows a minimum of two possible conformations: A folded and a stretched geometry, which we denote as conformers I and II, respectively. These result from an up or down location of the C_{60} moiety. In the folded geometry, small donor–acceptor separations are realized, see, for example, ZnP–BN–C_{60}. On the other hand, in the stretched geometry ZnP and C_{60} assume a maximum separation. In fact, molecular modeling on ZnP–BN–C_{60} and *ex*TTF–BN–C_{60} further supports this notion.

In the following discussion we will interpret the wire behavior observed in these systems, that is, electron conduction through the BN spacer, and compare this with our previous results with ZnP–wire–C_{60} and *ex*TTF–wire–C_{60} systems. These systems revealed charge-recombination dynamics in the range of $1.0\times10^6\ s^{-1}$ (THF)/$3.0\times10^6\ s^{-1}$ (benzonitrile) and $2.0\times10^6\ s^{-1}$ (THF)/$3.0\times10^6\ s^{-1}$ (benzonitrile) for the ZnP–wire–C_{60} and *ex*TTF–wire–C_{60} systems, respectively.[6a,7] Considering the dynamics in ZnP–BN–C_{60} one might anticipate, based on the short separation of 13.9 Å, molecular wire behavior. However, we concluded that the charge-transfer processes appear to be governed by through-space rather than through-bond interactions. This makes a conclusive interpretation difficult. More meaningful is the *ex*TTF–BN–C_{60} case, for which no evidence for through-bond interactions has been found. Here the deactivation dynamics (i.e., $1.6\times10^4\ s^{-1}$ in THF and $6.0\times10^3\ s^{-1}$ in benzonitrile) are several orders of magnitude lower than what would be expected for rapid charge mediation through the BN spacer over 16.6 Å. Consequently, we conclude that the integration of a simple C–C single bond breaks the electronic π conjugation in the BN spacer.

ZnP and *ex*TTF are both known as excellent electron donors. However, a number of fundamental differences in their chemical properties have been found. First, ZnP with its extended aromatic macrocycle forms tied packed π–π links with C_{60}, while the only aromatic parts in *ex*TTF are the benzenes in the anthracenoid subunit. Second, the planar structure of ZnP allows several short- and long-range interactions with the π system of C_{60}. Again *ex*TTF is different, its butterfly-type structure sterically limits the formation of a closely packed *ex*TTF/C_{60} structure. Thus, we conclude that conformer I is favored by ZnP–BN–C_{60} as a result of associative π–π interactions, which may be augmented to some extent by charge-transfer interactions. Experimental evidence for this hypothesis has come from electrochemical experiments and absorption spectroscopy. The reduced susceptibility of ZnP to oxidation and of C_{60} to reduction together with notable perturbations of the ground-state absorption features attest the electron-donor–electron-acceptor interactions. In *ex*TTF–BN–C_{60}, however, such an approach of donor (*ex*TTF) and acceptor (C_{60}) is hindered. In line with this assumption is the fact that the redox features are virtually unchanged relative to those of the individual components. On the other hand, broad absorptions hampered a meaningful analysis of the ground-state transitions.

Singlet excited-state deactivation sheds further light onto this phenomenon. For example, in fluorescence experiments, quenching of ZnP–BN–C_{60} is solvent-independent, which is an electron-transfer phenomenon typically found in flexibly spaced donor–acceptor ensembles. To activate intramolecular electron-transfer quenching in such flexible donor–acceptor systems, conformational prearrangements emerge as a necessary prerequisite. Governed by the driving forces outlined above, the donor and acceptor moieties must assume close contact with each other to facilitate exothermic electron transfer. Note that in **7**, additional complications may arise from the fact that energy and electron-transfer quenching compete with each other. Energy transfer between ZnP (2.1 eV) and C_{60} (1.76 eV) is exothermic and proceeds, in contrast to electron transfer, through a dipole–dipole mechanism. Despite this limitation, the fluorescence

experiments can be rationalized with reasonable confidence as a manifestation of intramolecular processes that occur preferentially in conformer I with a rate constant of $3.1 \pm 0.3 \times 10^9\ s^{-1}$.

In contrast to ZnP–BN–C_{60}, energy-transfer quenching between C_{60} (1.76 eV) and *ex*TTF (~2.9 eV) is thermodynamically impossible, which leaves electron-transfer quenching as the sole deactivation mechanism. The quenching in **6** cannot be rationalized entirely on the basis of differences in the free-energy changes of exothermic electron transfer. Based on this assumption one would expect increasing exothermicity from toluene through to benzonitrile, even though the absolute differences become somewhat marginal in polar solution. A realistic scenario involves a statistical distribution of conformers I and II. In fact, fluorescence lifetime profiles are best fitted with χ^2 values of ~1 when bi-exponential fitting functions are used. Typically, a short (i.e., ~0.2 ns) and long lifetime (i.e., ~0.9 ns) were noted. When comparing the data from experiments in toluene and THF, we see that the quantum yields decrease in parallel with the decrease in the relative weight of the long-lived component from 45 to 6%. In benzonitrile, the relative weight of the long-lived component went up again to around 50%.

More drastic are the effects seen on the stability of the charge-separated radical-ion pair. In both systems (i.e., ZnP–BN–C_{60} and *ex*TTF–BN–C_{60}) two radical-ion-pair products were seen. One of them decays virtually within a few microseconds, while the second one has lifetimes of up to 165 μs. In ZnP–BN–C_{60}, the product distribution is dominated (i.e., >95%) by the one formed via the short-lived radical-ion pair. *ex*TTF–BN–C_{60}, on the other hand, shows that up to 90% of the product originates from the long-lived radical ion pair.

However, it remains unclear at this stage which parameters, in addition to the dielectric constant, are responsible for the changes seen especially in *ex*TTF–BN–C_{60}.

Conclusions

To summarize, we have found that the topological effects of the geometrically well-defined chiral binaphthyl (BN) spacer play a leading role in electronic interactions in donor–acceptor ensembles. Thus, in ZnP–BN–C_6, associative π–π interactions augmented by charge-transfer interactions favor a conformer in which the ZnP is close to C_{60}, resulting in appreciable through-space electronic communication. In contrast, in *ex*TTF–BN–C_{60}, the lack of favorable interactions leads to two different conformers whose ratio depends on factors such as solvent polarity. As a result, strongly differing lifetimes were found for the photogenerated charge-separated states of the donor–acceptor ensembles: $ZnP^{\bullet+}$–BN–$C_{60}^{\bullet-}$: ~1 μs; *ex*$TTF^{\bullet+}$–BN–$C_{60}^{\bullet-}$: ~165 μs. Our study has provided an important strategy that allows the lifetime of charge-separated states to be controlled by means of topological effects, thus enabling new insights into photoinduced electron-transfer processes to be gained.

Experimental Section

General: FTIR spectra were recorded as KBr pellets with a Nicolet-Magna-IR 5550 spectrometer. Electrospray ionization (ESI) mass spectra were recorded with a HP1100MSD spectrometer. UV/Vis were recorded in dichloromethane in 1 cm quartz cuvettes with a Varian Cary 50 Scan spectrophotometer. NMR spectra were recorded with a Bruker AC-300 or Varian XL-300 (^{1}H: 300 MHz; ^{13}C: 75 MHz) spectrometer at 298 K using partially deuteriated solvents as internal standards. Chemical shifts are given as δ values (internal standard: TMS). Binaphthyl derivative **1**,[12] *ex*TTF **2**[11] and porphyrin **3**[13] were obtained by following previously described synthetic procedures. Elemental analyses were performed with Perkin-Elmer 2400 CHN and 2400 CHNS/O analysers. Tetrahydrofuran was dried with sodium.

Cyclic voltammograms were recorded with a potentiostat/galvanostat AUTOLAB with PGSTAT30 equipped with GPES for Windows version 4.8 software in a conventional three-compartment cell by using a GCE (glassy carbon electrode) as the working electrode, a SCE as the reference electrode, Bu_4NClO_4 as the supporting electrolyte, a *o*-dichlorobenzene/acetonitrile solvent mixture (4:1 v/v), and a scan rate of 200 $mV\,s^{-1}$.

Picosecond laser flash photolysis experiments were carried out with 355 or 532 nm laser pulses from a mode-locked, Q-switched Quantel YG-501 DP Nd:YAG laser system (18 ps pulse width, 2–3 mJ per pulse). Nanosecond laser flash photolysis experiments were performed with 355 or 532 nm laser pulses from a Quanta-Ray CDR Nd:YAG system (6 ns pulse width, 2 mJ per pulse) in a front-face excitation geometry. Concentrations of about 1.0×10^{-5} M were used, which rules out intermolecular or multiphoton processes. In fact, increasing or decreasing the concentration and/or laser energy by a factor of 2–3 led to notable differences.

Fluorescence lifetimes were measured with a Laser Strope Fluorescence Lifetime Spectrometer (Photon Technology International) with 337 nm laser pulses from a nitrogen laser fiber-coupled to a lens-based T-formal sample compartment equipped with a stroboscopic detector. Details of the Laser Strobe systems are described on the manufacture's website, http://www.pti-nj.com.

Emission spectra were recorded with a SLM 8100 spectrofluorimeter. The experiments were performed at room temperature. Each spectrum represents an average of at least 5 individual scans and appropriate corrections were applied whenever necessary.

Synthesis:

Compound 4: A mixture of the π-extended TTF derivative **2** (111 mg, 0.15 mmol) and potassium *tert*-butoxide (34 mg, 0.3 mmol) was refluxed in dry toluene under argon for 30 minutes. Once the formation of the ylide was completed, a solution of 2,2′-bis(dodecyloxy)-6,6′-diformyl-1,1′-binaphthalene (**1**) (170 mg, 0.25 mmol) in toluene (10 mL) was added dropwise and the mixture was further refluxed for 16 h. The crude product mixture was cooled to room temperature and CH_3OH (5 mL) was added. After evaporation of the solvents, the residue was purified by chromatography on silica gel with hexane/CH_2Cl_2 (3:2) as eluent to give the corresponding dyad. Unreacted binaphthyl derivative was also recovered. Yield: 51%. ^{1}H NMR (300 MHz, $CDCl_3$, 25°C, TMS): $\delta = 10.10$ (s, 1H), 8.36 (m, 1H), 8.11 (d, ^3J(H,H) = 9.0 Hz, 1H), 7.94 (d, ^3J(H,H) = 9.0 Hz, 1H), 7.89 (d, ^3J(H,H) = 11 Hz, 2H), 7.7 (m, 4H), 7.57 (m, 1H), 7.50 (d, ^3J(H,H) = 9.0 Hz, 2H), 7.40 (d, J = 9.0 Hz, 2H), 7.29 (m, 2H), 7.27 (d, ^3J(H,H) = 16.4 Hz, 1H), 7.14 (d, ^3J (H,H) = 16.4 Hz, 1H), 7.08 (d, J = 9.0 Hz, 1H), 6.31 (s, 4H), 3.97 (m, 4H), 1.43 (m, 4H), 1.3–0.9 (m, 36H), 0.89 (m, 6H) ppm; ^{13}C NMR (75 MHz, $CDCl_3$, 25°C, TMS): $\delta =$ 192.02, 157.30, 154.73, 137.59, 135.79, 135.71, 135.51, 135.30, 134.82, 134.56, 133.57, 132.62, 132.07, 131.05, 129.58, 129.34, 129.02, 128.88, 128.21, 127.97, 127.91, 127.78, 126.85, 126.48, 125.94, 125.49, 125.27, 124.92, 124.24, 124.12, 124.00, 123.12, 122.21, 122.14, 120.74, 119.62, 117.29, 117.19, 117.12, 115.86, 115.66, 69.49, 69.32, 31.92, 29.69, 29.65, 29.52, 29.48, 29.36, 29.30, 29.21, 29.11, 25.64, 22.69, 14.12 ppm; IR (KBr): $\tilde{\nu} =$ 2922, 2851, 1689, 1619, 1591, 1463, 1344, 1274, 1233, 1160, 1089, 1051, 961, 800, 754, 639 cm^{-1}; UV/Vis (CH_2Cl_2): λ_{max} ($\log \varepsilon / mol^{-1}\,cm^3\,dm^{-1}$) = 267 (5.05), 338 (4.91), 384 (4.81), 440 (4.72) nm; MS (ESI): m/z (%): 1054 (100) [M^+].

Compound 5: Potassium *tert*-butoxide (10 mg, 0.090 mmol) was added in portions to a refluxing solution of porphyrin **3** (40 mg, 0.047 mmol) and binaphthyl derivative **2** (64 mg, 0.094 mol) in dry THF (10 mL) under argon. The mixture was refluxed for 16 h and, after cooling to room temperature, a mixture of H_2O/MeOH (10 mL, 1:1) was added. The organic layer was separated and the aqueous layer was extracted with $CHCl_3$. The combined organic phases were washed with water and dried with $MgSO_4$. After evaporation of the solvent, the mixture was purified by chromatography on silica gel with hexane/ether (9:1) as eluent to give the corresponding dyad. Unreacted binaphthyl derivative was also recovered. Yield: 68%. ^{1}H NMR (300 MHz, $CDCl_3$, 25°C, TMS): δ = 10.12 (s, 1H), 9.00 (m, 8H), 8.24 (d, ^3J(H,H) = 8.0 Hz, 2H), 8.11 (m, 6H), 8.02 (d, ^3J(H,H) = 9.0 Hz, 2H), 7.92 (d, ^3J(H,H) = 8.0 Hz, 2H), 7.80 (m, 3H), 7.7–7.6 (m, 5H), 7.5–7.4 (m, 5H), 7.33 (d, ^3J(H,H) = 8.9 Hz, 1H) 7.19 (d, ^3J(H,H) = 8.9 Hz, 1H), 4.01 (m, 4H), 1.5–1.0 (m, 94H), 0.88 (m, 6H) ppm; ^{13}C NMR (75 MHz, $CDCl_3$, 25°C, TMS): δ = 192.09, 157.33, 154.80, 150.42, 150.37, 150.03, 148.52, 142.22, 141.80, 137.62, 136.62, 134.93, 134.79, 133.68, 132.71, 132.29, 132.22, 132.15, 132.08, 131.66, 131.10, 129.68, 129.58, 129.40, 129.35, 127.99, 127.88, 127.01, 126.52, 125.62, 124.62, 124.10, 123.14, 122.55, 122.46, 120.75, 120.43, 119.66, 115.86, 115.71, 69.51, 69.32, 35.03, 31.97, 31.95, 31.58, 31.53, 31.48, 31.40, 31.36, 31.34, 29.77, 29.68, 29.66, 29.59, 29.50, 29.43, 29.39, 29.32, 29.24, 29.18, 29.13, 25.68, 22.72, 14.15 ppm; IR (KBr): $\tilde{\nu}$ = 2953, 2925, 2855, 1694, 1619, 1592, 1437, 1362, 1247, 1000, 962, 822, 798 cm^{-1}; UV/Vis (CH_2Cl_2): λ_{max} ($\log\varepsilon$/mol^{-1} cm^3 dm^{-1}) = 269 (4.58), 293 (4.62), 331 (4.62), 403 (4.62, sh), 424 (5.67), 551 (4.32), 591 (3.86) nm. MS (ESI): *m*/*z* (%): 1688 (100) [M^+].

General procedure for the preparation of 6 and 7: A mixture of the corresponding dyad **4** or **5** (0.052 mmol), [60]fullerene (0.052 mmol), and *N*-octylglycine[28] (0.12 mmol) in chlorobenzene (28 mL) was refluxed for 24 h. After cooling to room temperature, the crude product mixture was purified by column chromatography on silica gel using CS_2 to elute the unreacted fullerene followed by hexane/toluene (1:1) to isolate the corresponding triad.

Compound 6: Yield: 37%. ^{1}H NMR (300 MHz, $CDCl_3$, 25°C, TMS): δ = 8.14 (m, 1H), 7.96 (d, ^3J(H,H) = 8.6 Hz, 1H), 7.88 (d, ^3J(H,H) = 8.6 Hz, 1H), 7.80 (m, 1H), 7.7–7.6 (m, 4H), 7.39 (m, 3H), 7.31 (d, ^3J(H,H) = 16.4 Hz, 1H), 7.30 (m, 1H), 7.26 (d, ^3J(H,H) = 16.4 Hz, 1H), 7.2–7.0 (m, 4H), 6.30 (s, 4H), 5.18 (s, 1H), 5.10 (d, ^3J(H,H) = 9.1 Hz, 1H), 4.14 (d, ^3J(H,H) = 9.1 Hz, 1H), 3.91 (m, 4H), 3.25 (m, 1H), 2.58 (m, 1H), 1,88 (m, 2H), 1.4–1.0 (m, 52H), 0.89 (m, 9H) ppm; ^{13}C NMR (75 MHz, $CDCl_3$, 25°C, TMS): δ = 156.66, 154.88, 153.80, 147.25, 146.99, 146.51, 146.37, 146.25, 146.19, 145.89, 145.74, 145.60, 145.55, 145.49, 145.44, 145.29, 145.23, 145.08, 144.70, 144.65, 144.57, 144.36, 143.17, 143.10, 142.95, 142.63, 142.52, 142.32, 142.29, 142.26, 142.13, 142.11, 142.07, 142.00, 141.93, 141.64, 141.50, 140.12, 140.07, 139.87, 139.29, 139.20, 136.64, 135.81, 135.76, 135.32, 134.50, 134.47, 134.29, 133.77, 133.67, 132.39, 129.42, 129.38, 129.24, 127.67, 126.91, 125.96, 125.27, 124.92, 122.15, 120.48, 118.34, 117.32, 117.19, 116.14, 82.72, 82.61, 69.77, 69.01, 66.89, 53.28, 31.99, 31.93, 31.90, 29.72, 29.70, 29.66, 29.64, 29.62, 29.59, 29.54, 29.43, 29.36, 29.31, 29.27, 29.16, 28.41, 27.61, 27.57, 25.73, 25.68, 25.65, 22.75, 22.71, 22.69, 14.19, 14.13 ppm; IR (KBr) $\tilde{\nu}$ = 2924, 2843, 1625, 1584, 1542, 1499, 1461, 1232, 1087, 799, 639, 527 cm^{-1}; UV/Vis (CH_2Cl_2): λ_{max} ($\log\varepsilon$/mol^{-1} cm^3 dm^{-1}) = 239 (5.19), 327 (4.79), 383 (4.58), 431 (4.44), 464 (4.25, sh) nm; MS (MALDI-TOF): *m*/*z* (%): 1899.6092 (100) [$M-H^-$]; calcd 1899.6038.

Compound 7: Yield: 47%. ^{1}H NMR (300 MHz, $CDCl_3$/CS_2, 25°C, TMS): δ = 8.97 (m, 8H), 8.21 (m, 2H,), 8.08 (m, 6H), 7.9–7.8 (m, 6H), 7.77 (m, 3H), 7.5–7.3 (m, 6H), 7.2–7.1 (m, 2H), 5.06 (m, 2H), 4.0–3.7 (m, 5H), 3.25 (m, 1H), 2.57 (m, 1H), 1.89 (m, 2H), 1.55 (s, 54H), 1.4–0.9 (m, 50H), 0.89 (m, 9H) ppm; ^{13}C NMR (75 MHz, $CDCl_3$/CS_2, 25°C, TMS): δ = 155.27, 155.15, 154.62, 154.04, 150.83, 150.80, 150.45, 148.82, 147.45, 147.27, 146.66, 146.56, 146.52, 146.33, 146.31, 146.17, 146.07, 146.06, 145.74, 145.58, 145.53, 145.46, 145.41, 145.37, 144.91, 144.64, 142.82, 142.72, 142.68, 142.60, 142.58, 142.36, 142.28, 142.22, 142.19, 142.07, 141.92, 141.87, 141.76, 140.33, 140.30, 139.65, 137.17, 137.14, 137.11, 135.38, 134.71, 134.32, 134.25, 133.02, 133.01, 132.96, 132.85, 132.81, 132.72, 132.64, 132.28, 132.24, 130.23, 130.15, 130.09, 129.96, 129.93, 129.88, 129.86, 129.80, 129.75, 129.72, 129.68, 129.63, 128.79, 128.23, 128.22, 127.60, 126.77, 126.69, 126.63, 125.14, 124.20, 122.90, 122.82, 121.23, 120.96, 120.94, 120.88, 120.84, 116.31, 116.22, 83.29, 70.10, 70.00, 69.97, 69.27, 35.38, 32.65, 32.25, 30.42, 30.33, 30.08, 29.92, 26.40, 23.52, 23.48, 14.88, 14.84 ppm; IR (KBr): $\tilde{\nu}$ = 2952, 2922, 2852, 1591, 1464, 1362, 1248, 1224, 1001, 799, 527 cm^{-1}; UV/Vis (CH_2Cl_2): λ_{max} ($\log\varepsilon$/mol^{-1} cm^3 dm^{-1}) = 235 (5.47), 307 (5.17), 329 (5.13), 402 (5.00, sh), 424 (6.00), 551 (4.69), 590 (4.28) nm; MS (ESI): *m*/*z* (%): 2555 (89) [M^+ +Na], 2532 (100) [M^+].

Acknowledgements

We thank the MCYT of Spain (Project BQU2002–00855) for financial support. Part of this work was carried out with partial support from the Deutsche Forschungsgemeinschaft (SFB 583), Fonds der chemischen Industrie, and the Office of Basic Energy Sciences of the U.S. Department of Energy. This is document NDRL-4619 from the Notre Dame Radiation Laboratory.

[1] a) *An Introduction to Molecular Electronics* (Eds.: M. C. Petty, M. R. Bryce, D. Bloor), Oxford University Press, New York, **1995**; b) *Molecular Electronics* (Eds.: J. Jortner, M. Ratner), Blackwell, Oxford, **1997**; c) M. A. Fox, *Acc. Chem. Res.* **1999**, *32*, 201–207; for a recent review on molecular electronics, see: d) R. L. Carroll, C. B. Gorman, *Angew. Chem. Int. Ed.* **2002**, *41*, 4378–4400.

[2] a) M. D. Ward, *Chem. Soc. Rev.* **1995**, *24*, 121–134; b) J. M. Tour, *Chem. Rev.* **1996**, *96*, 537–553; c) P. F. H. Schwab, M. D. Levin, J. Michl, *Chem. Rev.* **1999**, *99*, 1863–1933; d) R. E. Martin, T. Mäder, F. Diederich, *Angew. Chem.* **1999**, *111*, 834–838; *Angew. Chem. Int. Ed.* **1999**, *38*, 817; for a review on functionalized oligomers, see: e) J. L. Segura, N. Martín, *J. Mater. Chem.* **2000**, *10*, 2403–2435; f) J. M. Tour, *Acc. Chem. Res.* **2000**, *33*, 791–804; g) J. L. Segura, N. Martín, D. M. Guldi, *Chem. Soc. Rev.* **2005**, *34*, 31

[3] a) T. Gu, J.-F. Nierengarten, *Tetrahedron Lett.* **2001**, *42*, 3175–3178; b) T. Gu, D. Tsamouras, C. Melzer, V. Krasnikov, J.-P. Gisselbrecht, M. Gross, G. Hadziioannou, J.-F. Nierengarten, *ChemPhysChem* **2002**, *3*, 124–127; c) C. Atienza, B. Insuasty, C. Seoane, N. Martín, J. Ramey, D. M. Guldi, *J. Mater. Chem.* **2005**, *15*, 124–132.

[4] a) J. F. Nierengarten, J. F. Eckert, J. F. Nicoud, L. Ouali, V. Krasnikov, G. Hadziioannou, *Chem. Commun.* **1999**, 617–618; b) J. F. Eckert, J. F. Nicoud, J. F. Nierengarten, S. G. Liu, L. Echegoyen, F. Barigelletti, N. Armaroli, L. Ouali, V. V. Krasnikov, G. Hadziioannou, *J. Am. Chem. Soc.* **2000**, *122*, 7467–7479; c) N. Armaroli, F. Barigelletti, P. Ceroni, J.-F. Eckert, J.-F. Nicoud, J.-F. Nierengarten, *Chem. Commun.* **2000**, 599–600; d) E. Peeters, P. A. van Hal, J. Knol, C. J. Brabec, N. S. Sariciftci, J. C. Hummelen, R. A. J. Janssen, *J. Phys. Chem. B* **2000**, *104*, 10174–10190; e) J. L. Segura, R. Gómez, N. Martín, C. Luo, A. Swartz, D. M. Guldi, *Chem. Commun.* **2001**, 707–708; f) P. A. van Hal, R. A. J. Janssen, G. Lanzani, G. Cerullo, M. Zavelani-Rossi, S. De Silvestri, *Phys. Rev. B* **2001**, *64*, 075206–1–075206–7; g) N. Armaroli, G. Accorsi, J.-P. Gisselbrecht, M. Gross, M. V. Krasnikov, D. Tsamouras, G. Hadziioannou, M. J. Gómez-Escalonilla, F. Langa, J.-F. Eckert, J.-F. Nierengarten, *J. Mater. Chem.* **2002**, *12*, 2077–2087; h) J.-F. Nierengarten, N. Armaroli, G. Accorsi, Y. Rio, J.-F. Eckert, *Chem. Eur. J.* **2003**, *9*, 36–41; i) D. M. Guldi, C. Luo, A. Swartz, R. Gómez, J. L. Segura, N. Martín, C. Brabec, N. S. Sariciftci, *J. Org. Chem.* **2002**, *67*, 1141; j) D. M. Guldi, C. Luo, A. Swartz, J. L. Segura, R. Gómez, N. Martín, *J. Am. Chem. Soc.* **2002**, *124*, 10875.

[5] a) T. Benincori, E. Brenna, F. Sannicolo, L. Trimarco, G. Zotti, P. Sozzani, *Angew. Chem. Int. Ed. Engl.* **1996**, *35*, 648–651; b) F. Effenberger, G. Grube, *Synthesis* **1998**, 1372–1380; c) S. Knorr, A. Grupp, M. Mehring, G. Grube, F. Effenberger, *J. Chem. Phys.* **1999**, *110*, 3502–3508; d) T. Yamashiro, Y. Aso, T. Otsubo, H. Tang, Y. Harima, K. Yamashita, *Chem. Lett.* **1999**, 443–444; e) M. Fujitsuka, O. Ito, T. Yamashiro, Y. Aso, Y. Otsubo, *J. Phys. Chem. A* **2000**, *104*,

4876–4881; f) P. A. van Hal, J. Knol, B. M. W. Langeveld-Voss, S. C. J. Meskers, J. C. Hummelen, R. A. J. Janssen, *J. Phys. Chem. A* **2000**, *104*, 5974–5988; g) P. A. van Hal, R. A. J. Janssen, G. Lanzani, G. Cerullo, M. Zavelani-Rossi, S. De Silvestri, *Chem. Phys. Lett.* **2001**, *345*, 33–38; h) M. Fujitsuka, A. Masahura, H. Kasai, H. Oikawa, H. Nakanishi, O. Ito, T. Yamashiro, Y. Aso, T. Otsubo, *J. Phys. Chem. B.* **2001**, *105*, 9930–9934; i) D. Hirayama, K. Takimiya, Y. Aso, T. Otsubo, T. Hasobe, ; H. Yamada, H. Imahori, S. Fukuzumi, Y. Sakata, *J. Am. Chem. Soc.* **2002**, *124*, 532–533; j) N. Negishi, K. Yamada, K. Takimiya, Y. Aso, T. Otsubo, Y. Harima, *Chem. Lett.* **2003**, *32*, 404–405.

[6] a) J. M. Tour, A. M. Rawlett, M. Kozaki, Y. Yao, R. C. Jagessar, S. M. Dirk, D. W. Price, M. A. Reed, C.-W. Zhou, J. Chen, W. Wang, I. Campbell, *Chem. Eur. J.* **2001**, *7*, 5118–5134; b) I. Jestin, P. Frère, P. Blanchard, J. Roncali, *Angew. Chem.* **1998**, *110*, 990–993; *Angew. Chem. Int. Ed.* **1998**, *37*, 942–945.

[7] a) F. Giacalone, J. L. Segura, N. Martín, D. M. Guldi, *J. Am. Chem. Soc.* **2004**, *126*, 5340–5341; b) F. Giacalone, N. Martín, J. Ramey, D. M. Guldi, *Chem. Eur. J.* **2005**, *11*, 4819–4834.

[8] G. De la Torre, F. Giacalone, J. L. Segura, N. Martín, D. M. Guldi, *Chem. Eur. J.* **2005**, *11*, 1267–1280.

[9] L. Pu, *Chem. Rev.* **1998**, *98*, 2405–2494.

[10] R. Gómez, J. L. Segura, N. Martín, *Chem. Commun.* **1999**, 619–620.

[11] M. Otero, M. A. Herranz, C. Seoane, N. Martín, J. Garín, J. Orduna, R. Alcalá, B. Villacampa, *Tetrahedron* **2002**, *58*, 7463–7475.

[12] R. Gómez, J. L. Segura, N. Martín, *J. Org. Chem.* **2000**, *65*, 7501–7511.

[13] X. J. Salom-Roig, J.-C. Chambron, C. Goze, V. Heitz, J.-P. Sauvage, *Eur. J. Org. Chem.* **2002**, *67*, 3276–3280.

[14] These systems (exTTF–BN–exTTF and ZnP–BN–ZnP) can be prepared in larger amounts by controlling the stoichiometry of the reactants. The synthesis and characterization of these compounds will be reported elsewhere.

[15] a) M. Maggini, M. Prato, G. Scorrano, *J. Am. Chem. Soc.* **1993**, *115*, 9798–9799; b) M. Prato, M. Maggini, *Acc. Chem. Res.* **1998**, *31*, 519–526; c) N. Tagmatarchis, M. Prato, *Synlett*, **2003**, 768–779.

[16] a) L. Echegoyen, L. E. Echegoyen, *Acc. Chem. Res.*, **1998**, *31*, 593–601; b) N. Martín, L. Sánchez, B. Illescas, I. Pérez, *Chem. Rev.* **1998**, *98*, 2527–2548.

[17] a) F. D′Souza, G. R. Deviprasad, M. E. El-Khouly, M. Fujitsuka, O. Ito, *J. Am. Chem. Soc.* **2001**, *123*, 5277–5284; b) F. D′Souza, G. R. Deviprasad, M. E. Zandler, V. T. Hoang, A. Klykov, M. VanStipdonk, A. Perera, M. E. El-Khouly, M. Fujitsuka, O. Ito, *J. Phys. Chem. A.* **2002**, *106*, 3243–3252; c) F. Fungo, L. Otero, C. D. Borsarelli, E. N. Durantini, J. J. Silber, L. Sereno, *J. Phys. Chem. B.* **2002**, *106*, 4070–4078; d) F. D′Souza, G. R. Deviprasad, M. E. Zandler, M. E. El-Khouly, M. Fujitsuka, O. Ito, *J. Phys. Chem. B.* **2002**, *106*, 4952–4962.

[18] E. Díez-Barra, J. C. García-Martínez, R. del Rey, J. Rodríguez-López, F. Giacalone, J. L. Segura, N. Martín, *J. Org. Chem.* **2003**, *68*, 3178–3183.

[19] F. D′Souza, G. R. Deviprasad, M. E. Zandler, M. E. El-Khouly, M. Fujitsuka, O. Ito, *J. Phys. Chem. A* **2003**, *107*, 4801–4807.

[20] a) D. M. Guldi, M. Scheloske, E. Dietel, A. Hirsch, A. Troisi, F. Zerbetto, M. Prato, *Chem. Eur. J.* **2003**, *9*, 4968–4979; b) D. M. Guldi, C. Luo, A. Swartz, M. Scheloske, A. Hirsch, *Chem. Commun.* **2001**, 1066; c) D. M. Guldi, C. Luo, M. Prato, A. Troisi, F. Zerbetto, M. Scheloske, E. Dietel, W. Bauer, A. Hirsch, *J. Am. Chem. Soc.* **2001**, *123*, 9166.

[21] J. L. Segura, N. Martín, *Chem. Rev.* **1999**, *99*, 3199–3246.

[22] D. M. Guldi, *Chem. Soc. Rev.* **2002**, *31*, 22–36.

[23] D. M. Guldi, M. Prato, *Acc. Chem. Res.* **2000**, *33*, 695–703.

[24] J. Rodriguez, C. Kirmaier, D. Holten, *J. Am. Chem. Soc.* **1989**, *111*, 6500–6506.

[25] a) H. Imahori, K. Hagiwara, M. Aoki, T. Akiyama, S. Taniguchi, T. Okada, M. Shirakawa, Y. Sakata, *J. Am. Chem. Soc.* **1996**, *118*, 11771–11782; b) H. Imahori, K. Tamaki, D. M. Guldi, C. Luo, M. Fujitsuka, O. Ito, Y. Sakata, S. Fukuzumi, *J. Am. Chem. Soc.* **2001**, *123*, 2607; c) D. M. Guldi, K. Tamaki, Y. Yoshida, C. Luo, Y. Sakata, S. Fukuzumi, *J. Am. Chem. Soc.* **2001**, *123*, 6617; d) H. Imahori, H. Yamada, D. M. Guldi, Y. Endo, A. Shimomura, S. Kundu, K. Yamada, T. Okada, Y. Sakata, S. Fukuzumi, *Angew. Chem.* **2002**, *114*, 2450; *Angew. Chem. Int. Ed.* **2002**, *41*, 2344; e) S. Fukuzumi, K. Ohkubo, H. Imahori, D. M. Guldi, *Chem. Eur. J.* **2003**, *9*, 1585

[26] D. M. Guldi, H. Hungerbühler, K.-D. Asmus, *J. Phys. Chem.* **1995**, *99*, 9380–9385.

[27] D. M. Guldi, L. Sánchez, N. Martín, *J. Phys. Chem. B* **2001**, *105*, 7139–7144.

[28] C. M. Deber, P. D. Adawadkar, *Biopolymers* **1979**, *18*, 2375–2396.

Received: February 24, 2005
Revised: May 13, 2005
Published online: September 15, 2005

